Delft University of Technology

Optical Switching of Hole Transfer in Double-Perovskite/Graphene Heterostructure

Zhang, Heng; Debroye, Elke; Fu, Shuai; González, Miriam C.Rodriguez; du Fossé, Indy; Geuchies, Jaco J.; Gao, Lei; Yu, Xiaoqing; Houtepen, Arjan J.; More Authors

Important note
To cite this publication, please use the final published version (if applicable).
Please check the document version above.

Optical Switching of Hole Transfer in Double-Perovskite/Graphene Heterostructure

Heng Zhang, Elke Debroye, Shuai Fu, Miriam C. Rodriguez González, Indy du Fossé,
Jaco J. Geuchies, Lei Gao, Xiaoqing Yu, Arjan J. Houtepen, Steven De Feyter,
Johan Hofkens, Mischa Bonn, and Hai I. Wang**

Synergically combining their respective ultrahigh charge mobility and strong light absorption, graphene (Gr)/semiconductor heterostructures are promising building blocks for efficient optoelectronics, particularly photodetectors. Charge transfer (CT) across the heterostructure interface crucially determines device efficiency and functionality. Here, it is reported that hole-transfer processes dominate the ultrafast CT across strongly coupled double-perovskite $Cs_2AgBiBr_6$/graphene (DP/Gr) heterostructures following optical excitation. While holes are the primary charges flowing across interfaces, their transfer direction, as well as efficiency, show a remarkable dependence on the excitation wavelength. For excitation with photon energies below the bandgap of DPs, the photoexcited hot holes in Gr can compete with the thermalization process and inject into in-gap defect states in DPs. In contrast, above-bandgap excitation of DP reverses the hole-transfer direction, leading to hole transfer from the valence band of DPs to Gr. Experimental evidence that increasing the excitation photon energy enhances CT efficiency for both below- and above-bandgap photoexcitation regimes is further provided, unveiling the positive role of excess energy in enhancing interfacial CT. The possibility of switching the hole-transfer direction and thus the interfacial photogating field by tuning the excitation wavelength, provides a novel way to control the interfacial charge flow across a DP/Gr heterojunction.

1. Introduction

Graphene (Gr)/semiconductor heterostructures have emerged as promising building blocks for optoelectronics due to the unique combination of ultrahigh charge mobility in Gr

($>10^5$ cm^2 V^{-1} s^{-1})[1,2] and the strong optical absorption of semiconductors.[3] In particular, efficient conversion of light to electrical signals in photodetectors, has been experimentally demonstrated in Gr-based heterostructures with various types of semiconductors as light absorbers, including colloidal quantum dots,[4] nanographenes,[5] 2D transition metal dichalcogenides (TMDs),[6] and bulk crystalline materials.[7] Fundamentally, the device performance critically relies on both the charge transfer (CT) and recombination processes (i.e., back-CT) across the hybrid interfaces. While the former determines the population of charge carriers across the interfaces (i.e. the CT efficiency), the latter impacts the duration of the interfacial electrical field induced by the charge separation that gates or modulates the conductivity of Gr: the longer the charge separation, the higher the photoconductive gain for the light detection (so-called "photogating" mechanism).[4]

From this perspective, understanding and eventually achieving complete control of interfacial charge carrier dynamics, for example, the charge separation pathways and efficiency, the direction of the interfacial gating field, as well as the lifetime of charge separation, are of fundamental significance for improving the photodetection capabilities of Gr-based heterostructures. Combining terahertz (THz) and transient absorption (TA)

H. Zhang, S. Fu, J. J. Geuchies, L. Gao, X. Yu, M. Bonn, H. I. Wang
Max Planck Institute for Polymer Research
Ackermannweg 10, 55128 Mainz, Germany
E-mail: wanghai@mpip-mainz.mpg.de

E. Debroye, M. C. R. González, S. De Feyter, J. Hofkens
Department of Chemistry
KU Leuven
Celestijnenlaan 200F, Leuven 3001, Belgium
E-mail: elke.debroye@kuleuven.be

I. du Fossé, A. J. Houtepen
Optoelectronic Materials Section
Faculty of Applied Sciences
Delft University of Technology
Delft 2629HZ, The Netherlands

L. Gao
School of Physics and Key Laboratory of MEMS of the Ministry of Education
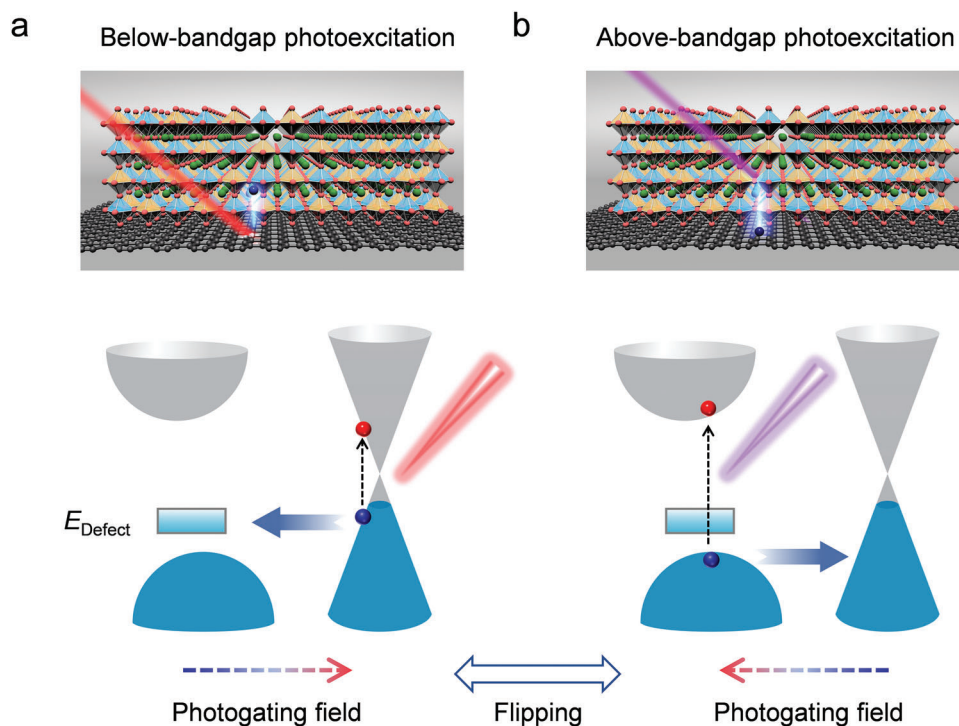Southeast University
Nanjing 211189, China

Figure 1. Schematic illustration of the optically controlled hole-transfer dynamics in a DP/Gr heterostructure in both real (top) and momentum (bottom) spaces. a) Upon excitation with photon energies below the bandgap of DP, the photoexcited hot holes in Gr are transferred to the DP. b) For photoexcitation with photon energies above the bandgap of DP, hole transfer from the DP to Gr dominates the transfer process. The rectangles in the lower panel represent the filled defect states in $Cs_2AgBiBr_6$.

spectroscopies, Fu et al. investigated the ultrafast CT processes across Gr/WS_2 heterostructures by varying the laser excitation photon energies.[8] They showed that both the CT pathways and efficiency can be controlled by photoexcitations: when only Gr is excited, initial "nascent" hot carriers can effectively transfer energy to charge carriers at the Fermi surface via carrier–carrier scattering. This results in the generation of hot carriers following a Fermi–Dirac distribution with high electronic temperature (e.g., over 1000 K). Following this "thermalization" (or carrier heating) process, energetic hot electrons can be emitted over the interfacial energy barrier and injected into the conduction band of WS_2, the so-called photo-thermionic emission. On the other hand, direct excitation of the WS_2 layer results in the transfer of "cold" electrons from the valence band of Gr to the photogenerated hole states in the valence band of WS_2, which is equivalent to a hole-transfer process from WS_2 to Gr. Such an interfacial CT mechanism has also been reported by photocurrent measurements[9] and TA spectroscopy.[10] While the excitation condition can modulate the CT pathways and efficiency, the direction of photoinduced CT is fixed. In the case of Gr/WS_2, Gr loses electrons to WS_2 across the entire excitation wavelength range. The realization of switching the CT direction by external stimuli can provide a novel degree of freedom to tune the direction of the local gating field for light detection applications.

In the last decade, the world has witnessed the rapid rise of low-temperature solution-processed lead halide perovskites (LHPs) as one of the most cost-effective optical absorbers for photovoltaics with the record light-to-electricity power conversion efficiency of more than 25% for single-junction solar cells.[11,12]

Gr/LHP heterostructures have also been explored and shown superior photodetection performance with an ultra-broadband photoresponse and ultrahigh photoresponsivity.[13,14] However, the lead toxicity and chemical instability of LHPs have largely impeded their practical applications and commercialization. By alternatively substituting two bivalent lead cations Pb^{2+} with one mono- $([B']^+)$ and one trivalent $([B'']^{3+})$ metal cation, the so-called double perovskite (DP) with the chemical formula $A_2B'B''X_6$ has been successfully synthesized with extraordinary chemical stability and optoelectronic properties. Among them, one of the most promising DPs is the all-inorganic $Cs_2AgBiBr_6$ featuring strong optical absorption (from the UV–vis to the X-ray spectral range),[15–17] long carrier lifetime,[18–20] and large carrier diffusion length.[21] Characterization of interfacial electronic coupling and CT dynamics in DP/Gr heterostructures is crucial to provide fundamentals for realizing high-performance optoelectronics (e.g., broadband photodetectors from the infrared to the UV range) and for exploring new functionalities, for example, new device schemes for X-ray detection.

In this work, we investigate the interlayer electronic coupling and photoinduced CT processes in a DP/Gr heterostructure combining Raman spectroscopy, Kelvin probe force microscopy (KPFM), and ultrafast time-resolved THz spectroscopy. We report that the hole transfer across the interface dominates the CT processes following photoexcitation, and its direction critically relies on the excitation photon energy. As illustrated schematically in **Figure 1**, when the photon energy is below the bandgap of the DP (i.e., only the Gr layer is excited), the photoexcited hot holes in Gr are transferred to the DP. On the other hand, when the
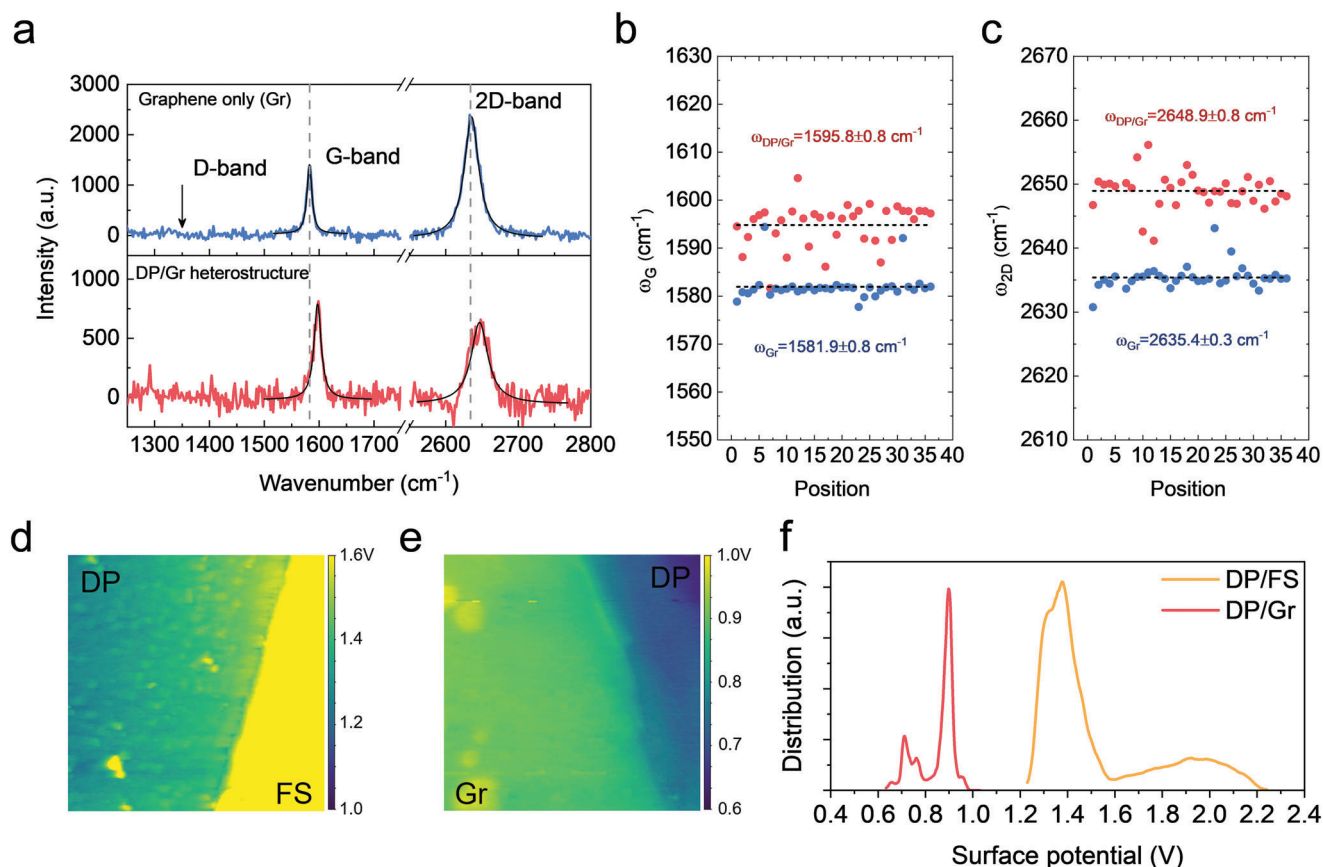
ADVANCED
SCIENCE NEWS
www.advancedsciencenews.com

ADVANCED
MATERIALS
www.advmat.de

Figure 2. Characterization of the DP/Gr interlayer electronic coupling by Raman spectroscopy and KPFM. a) Raman spectra of pure Gr (top) and the DP/Gr heterostructure (bottom). The solid black lines represent the Lorentz peak fits. b,c) Spatial mapping of the G-band (b) and 2D-band (c) within an area of 1 mm × 1 mm for pure Gr and DP/Gr. The dashed lines represent the average values for each data set. d,e) Surface potential images of DP on a fused silica substrate (DP/FS) (d) and DP on Gr (DP/Gr) (e). f) Distribution of the surface potential of DP/FS and DP/Gr.

heterostructure is excited by photons with an energy higher than the bandgap of the DP, the hole-transfer direction is reversed, taking place from the valence band of the DP to Gr. The transition in the hole-transfer direction results in the flipping of the photogating electric field, as well as in a change of the interlayer charge carrier recombination pathway and thus time. Furthermore, by increasing the energy of the photoinjected holes (by increasing the excitation photon energy), the hole-transfer efficiency is enhanced in both below- and above-bandgap photoexcitation regimes. The unique directional switching of hole transfer and its efficiency modulation by varying the optical excitation provides a novel knob to control the interfacial charge flows in a Gr-based heterostructure for novel optoelectronic device design.

2. Results and Discussion

2.1. Strong DP/Gr Interlayer Coupling Revealed by Raman Spectroscopy and KPFM

Strong interlayer electronic coupling is required to achieve highly efficient CT across the hybrid interface following optical excitation. We first characterize the electronic coupling of the DP/Gr heterostructure at their static charge equilibrium (i.e., without photoexcitation) by combining Raman spectroscopy and KPFM.

While the Fermi energy E_F of Gr can be readily monitored by Raman spectroscopy, the surface potential and thus the work function of the DP can be tracked by KPFM.

As shown in **Figure 2**a, two characteristic Raman modes centered at around 1580 and 2650 cm^{-1} in bare Gr are assigned to the G-band and 2D-band.[22,23] The absence of layer-breathing modes at around 1500 and 1740 cm^{-1} is indicative of monolayer Gr.[22] In addition, there is no defect-activated D-band ($\approx$1350 cm^{-1}) observed in the Gr layer before and after the DP deposition,[22] indicating that the high-quality Gr monolayer was preserved following a mild UV–ozone treatment (with an O_2 injection rate of 0.2 L min^{-1}) and DP deposition (see the sample preparation in the Experimental Section). In line with this claim, we find that the graphene's photoconductivity dynamics and thus its electrical properties remain almost the same following mild UV–ozone treatments (see the result in the Supporting Information). Upon the deposition of DP onto Gr, both the G-band and 2D-band of Gr are blue-shifted relative to pure Gr, which is statistically confirmed in Figure 2b,c by scanning an area of 1 mm × 1 mm. G-band and 2D-band positions are reported to be sensitive to the carrier density and charge species (i.e., electron or hole) in Gr.[22,23] While the blue-shifted G-band implies an increase in the total charge carrier density, the blue shift of the 2D-band indicates a hole population increase in Gr.[23] Given the initial p-doping
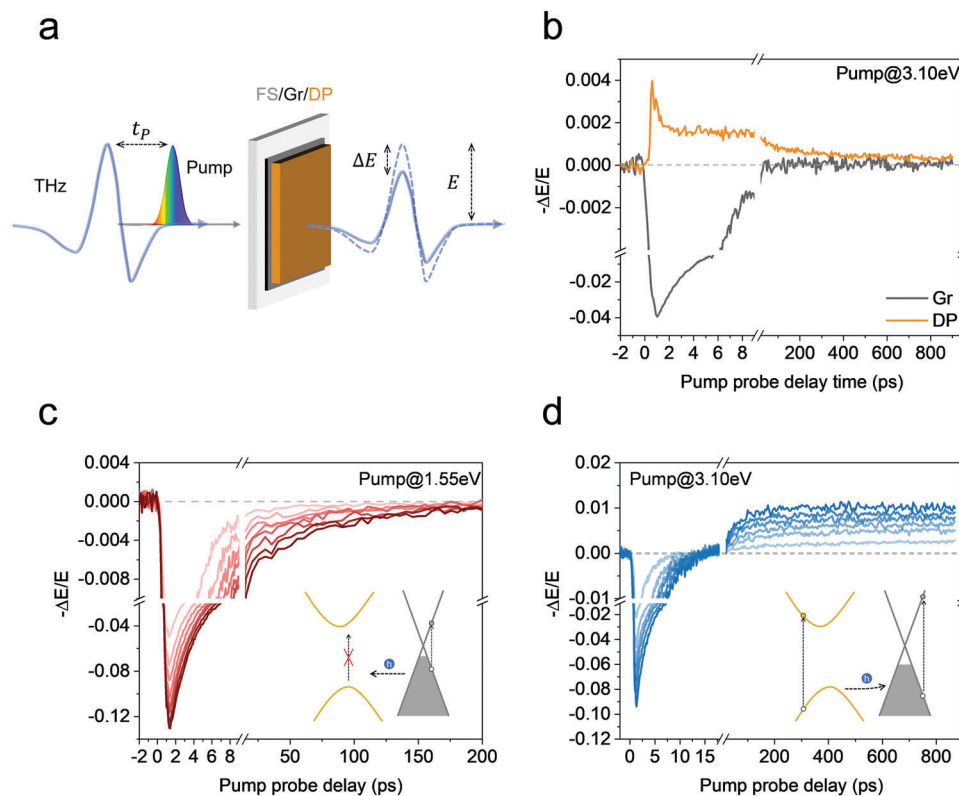
Figure 3. Photoinduced charge transfer in DP/Gr heterostructures. a) Schematic of OPTP measurements. b) The OPTP dynamics for pure graphene (Gr, gray line) and double perovskite (DP, yellow line), pumped with a 400 nm (photon energy of 3.10 eV) laser pulse at a fixed fluence of 60.9 μJ cm^{-2} at room temperature. c) Fluence-dependent OPTP dynamics for the DP/Gr heterostructure upon 800 nm (photon energy of 1.55 eV) photoexcitation. The fluence increases from 24.5 to 233 μJ cm^{-2}. d) Fluence-dependent OPTP dynamics for the DP/Gr upon 3.10 eV photoexcitation. The fluence increases from 9.8 to 147 μJ cm^{-2}.

nature of chemical vapor deposited (CVD-grown) Gr transferred onto fused silica (FS) substrates,[8,24] the Raman results indicate that the Fermi level E_F of Gr shifts downwards, further away from the Dirac point, by losing electrons to the DP. Employing the empirical relation between the G-band positions and the Fermi energy E_F:[23] $\omega_G - 1580 \, \text{cm}^{-1} = 42 \, \text{cm}^{-1} \text{eV}^{-1} \cdot |E_F|$, we estimate that the E_F shifts substantially over 330 meV from −50 to −380 meV below the Dirac point. According to the relation between E_F and charge density N: $|E_F| = \hbar v_F (\pi |N|)^{1/2}$ ($\hbar$ is the reduced Planck constant, v_F is the Fermi velocity),[8] the hole density increases from 1.24×10^{11} to 8.59×10^{12} cm^{-2}. The electron flow from Gr to the DP (which results in strong hole doping in Gr) inferred from Raman spectroscopy is further corroborated by KPFM measurements. Figure 2d–f shows the mapping and distribution of the surface potential of DP deposited on either fused silica (DP/FS) or graphene (DP/Gr). As we can see, in both cases the values obtained for the area covered by the perovskite film is lower than in the case of the bare substrate. The topography of the sample was registered simultaneously to the mapping of the surface potential (Figure S1, Supporting Information), showing a thickness of around 100–200 nm for both films. In Figure 2f we can observe the distribution of the surface potential of the DP in DP/Gr and DP/FS samples. Clearly, the surface potential for the DP/Gr sample is shifted to lower values when compared to the DP/FS sample. Based on this result, we conclude that the surface potential

and thus the work function of DP on Gr is reduced in comparison to the DP on insulating silica substrates, that is, the Fermi level in DP increases following an interfacial charge equilibrium. Given the large amount of charge flow across the DP/Gr interface, the combined Raman and KPFM studies indicate a strong interfacial electronic coupling.

2.2. Optical Switching of Hole Transfer across DP/Gr Interfaces

To unveil the photoinduced CT dynamics in DP/Gr heterostructures, we employ contact-free, optical pump–THz probe (OPTP) spectroscopy as depicted in **Figure 3**a with sub-picosecond (ps) time resolution.[8,25] In the OPTP measurement, we photogenerate charge carriers in materials by above-bandgap-energy (E_g) excitations. Subsequently, a single-cycle THz pulse probes the photoconductivity ($\Delta\sigma$) of the sample; the photogenerated free carriers absorb THz field E, which leads to attenuation of the field by an amount of ΔE. The relative change of the electric field $-\Delta E/E$ is proportional to $\Delta\sigma$ ($= \sigma_{pump} - \sigma_0$), σ_0 and σ_{pump} are the conductivity without and with photoexcitation).[25] The delay time between the pump and probe pulses t_p is controlled by an optical delay line. OPTP spectroscopy for tracking the CT processes across Gr-based heterostructures relies on Gr's extremely high charge

**ADVANCED
SCIENCE NEWS**

www.advancedsciencenews.com

**ADVANCED
MATERIALS**

www.advmat.de

carrier mobility. This leads to a substantial change in conductivity upon electron gain or loss (ΔN) in Gr following CT.[5,8,26]

We first characterize the photoconductivity response from the individual layers under the same pump photon energy of 3.10 eV (exceeding the indirect bandgap energy of DP with $E_g \approx 2.17$ eV) and the same pump fluence of 60.9 µJ cm^{-2}. As shown in Figure 3b, photoexcitation of Gr results in a transient reduction in conductivity, that is, negative photoconductivity. Such observation has been well documented previously for doped Gr, and the reduced conductivity is assigned to the mobility decrease of charge carriers[27,28] due to the generation of thermalized hot carriers. Hot carriers have been reported to be electrostatically less screened than cold ones, resulting in much enhanced scattering effects to, for example, the charged impurities in the substrate.[29] After hot-carrier cooling within several ps,[30] the electronic system returns to the initial equilibrium condition. The hot-carrier cooling time does not depend on the pump photon energy (see Figure S3, Supporting Information, for comparing photoconductivity of bare Gr following photoexcitation at 1.55 and 3.10 eV photons). On the other hand, photoexcitation into the DP results in the generation of free carriers and thus positive photoconductivity. In line with our results, the long-lived carrier lifetime of more than 1 µs in Cs$_2$AgBiBr$_6$ has been previously reported.[19] Note here that, owing to the much higher charge carrier mobility, the absolute value of photoconductivity in bare Gr is almost an order of magnitude larger than that for the bare DP for the same pump fluence, despite the much lower absorption of Gr.[8,25] For the same reason, the Gr's conductivity change following optical excitation and interfacial CT is expected to dominate the photoresponse of the system and can be used as a sensitive probe to track the CT processes across the DP/Gr interface.

To unveil the CT pathways and mechanisms, we conduct pump photon energy- and fluence-dependent OPTP measurements to the strongly coupled DP/Gr hybrids. In Figure 3c,d, we present the fluence-dependent OPTP dynamics upon 1.55 and 3.10 eV photoexcitation as two exemplary photon energies. These two excitation wavelengths are judiciously chosen to represent and compare the dynamics upon excitation below and above the E_g of the DP. In both cases, the photoresponse of Gr dominates at the early time, that is, the short-lived negative photoconductivity in the first few ps. On the other hand, the sign of the long-lived photoconductivity (10 ps and beyond after photoexcitation) is affected by CT and critically depends on the pump-photon energy: for below-E_g excitation in Figure 3c, that is, when only Gr is excited, we observe a negative photoconductivity with a decay time of over 100 ps, substantially longer than the sub-10 ps hot-carrier cooling time in bare Gr. Considering the initial strong p-doping of Gr in contact with DP, the long-lived negative photoconductivity indicates a hole loss (or, equivalently, electron gain) in the Gr layer: that is, a hole-transfer process from Gr to DP. In stark contrast, above-E_g excitation leads to a long-lived positive photoconductivity of which the intensity increases with increasing excitation fluence, as shown in Figure 3d. Due to the increased lifetime and much higher intensity compared to the signal of bare DP (see Figure S4, Supporting Information, for the direct comparison of OPTP dynamics at the same fluence for DP, Gr, and DP/Gr), we confirm the long-lived positive photoconductivity stems mainly from the CT-induced conductivity changes in Gr. Furthermore, the positive photoconductivity implies a hole gain process in Gr,

i.e., photogenerated hole transfer from the valence band of the DP to the valence band of Gr. Therefore, the results presented in Figure 3c,d unveil a remarkable transition in the hole-transfer direction, from a Gr-to-DP hole transfer for below-E_g excitation to a DP-to-Gr hole transfer for above-E_g excitation. Furthermore, we confirm that the direction and efficiency of CT in DP/Gr do not depend on the excitation direction (from Gr or DP side; see Figure S6, Supporting Information).

To further corroborate the switching in the hole-transfer direction by exciting the heterostructure across the E_g of the DP and shed light on the states involved in the CT mechanism, we conducted wavelength- and fluence-dependent photoconductivity for seven different excitation wavelengths covering a wide range from 1.20 to 3.65 eV (see Figure S7, Supporting Information). **Figure 4**a shows the OPTP dynamics for a given absorbed photon density for all excitation wavelengths. We summarize the fluence-dependent CT-induced photoconductivities in Figure 4b. For the long-lived negative photoconductivity (below-E_g photoexcitation), we take the values at a pump–probe delay time of 50 ps to ensure zero contribution from the intrinsic hot-carrier dynamics from Gr (which should have decayed within 10 ps). For the long-lived positive photoconductivity (above-E_g photoexcitation), we extract the value at 800 ps. We further define the efficiency by the slope in the fluence-dependent photoconductivity plot as shown in Figure 4b, and summarize the result in Figure 4c. For above-E_g excitation, due to the sublinear dependence between the photoconductivity and fluence, we approximate the efficiency by a linear fit to the first three data points (including (0, 0)) in the low fluence regime. The sublinear dependence at increased fluence may be attributed to enhanced charge recombination in DPs due to, for example, Auger recombination. While such estimation apparently overestimates the CT efficiency in the high-fluence range, our conclusion of hole-transfer direction flip does not depend on the fluence range included for the CT efficiency estimation.

As we can see in Figure 4, there is a clear sudden transition in the long-lived photoconductivity from negative to positive by increasing the energy of pump photons. This sharp transition occurs precisely at the bandgap of DPs. These data directly support our claim of hole-transfer direction switching as the photon energy is tuned across the bandgap of the DP. To the best of our knowledge, this observation represents the first realization of controlling the CT direction in heterostructures by external stimuli, for example, excitation by photons of different energies in this study. More importantly, the switching of the hole-transfer direction implies a flipping of the photogating field at interfaces, which could profoundly impact the photodetection mechanism in DP/Gr.

Next, we discuss the states involved and corresponding CT times in the two hole-transfer regimes. First, for above-E_g excitation, as holes are mainly photogenerated in the valence band of the DP, it is obvious that the hole transfer takes place from the valence band of DP to the valence band of Gr. For the CT time, the hot-carrier response in Gr masks the signal from fast injection channels, which makes it challenging to infer the CT rate and weight in the early time scale. We notice a "slow" injection channel with an injection time of ≈ 100 ps (e.g., for 2.43 and 3.10 eV; see Supporting Information for discussion). This injection channel may originate from the convoluted diffusion and injection
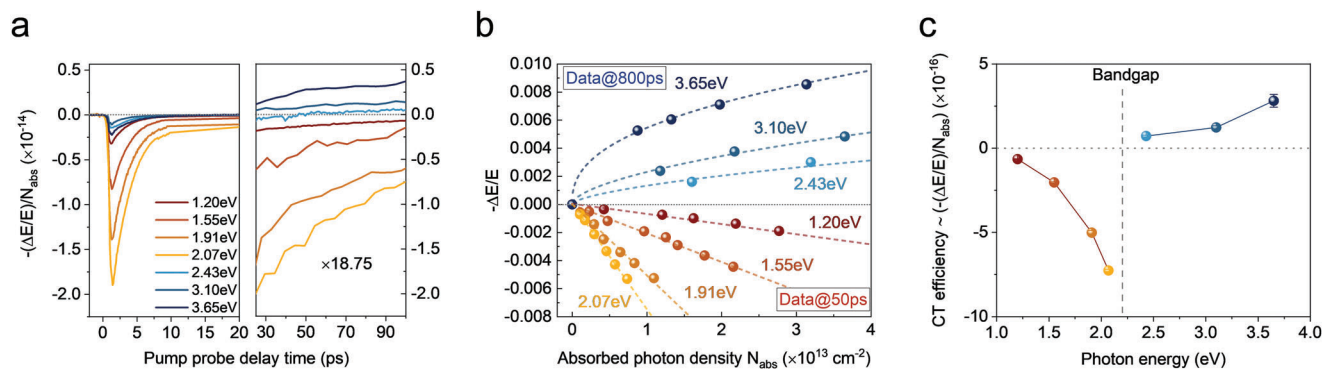
ADVANCED
SCIENCE NEWS

www.advancedsciencenews.com

ADVANCED
MATERIALS

www.advmat.de

Figure 4. Photon energy- and fluence-dependent charge transfer in DP/Gr heterostructure. a) OPTP dynamics normalized to the absorbed photon density at different pump photon energies. The left and right panels show the dynamics in different time delay windows. The data in the right panel are multiplied by a factor ≈ 19 for better visualization. b) OPTP signal as a function of the absorbed photon density for different pump photon energies. For photon energies below the bandgap of DP, the data points are extracted at a pump–probe delay time of 50 ps; for photon energies above the bandgap of DP, the data are taken at 800 ps after photoexcitation. The dashed lines are guides to the eye. c) The relative CT efficiencies (proportional to $-(\Delta E/E)/N_{abs}$) as a function of pump photon energy. The vertical dashed line indicates the bandgap of DP.

dynamics for charge carriers generated in the DP far from the interface.[31] Second, for below-E_g excitations, there is no clear indication of the nature of the accepting states in the DP (the valence band or defect states), and whether thermalized (e.g., via photo-thermionic emission[9]) or non-thermalized hot Gr holes are involved in the transfer. First, we can rule out the injection of thermalized hot holes from Gr to DP as the main CT mechanism. In that case, the energetic thermalized hot carriers (following the Fermi–Dirac distribution) with energies beyond the Schottky barrier can be emitted from Gr to DP. A superlinear dependence between the CT efficiency and excitation fluence is expected for such a "photo-thermionic emission" picture[8,9] which is in contrast to the observed linear dependence in Figure 4b. As such, we conclude that in the below-E_g excitation regime, transfer of non-thermalized hot holes dominates the CT process. For this scenario, CT can take place only when the excess energy of "nascent" hot holes in Gr exceeds the interfacial Schottky energy barrier. By considering the rate competition between the thermalization (within 100 fs) and the CT, the CT time needs to be in the sub-ps time scale to ensure sufficiently high CT efficiency (>8% in this case; see discussion in following section). Based on the energetics of the DP and Gr, the Schottky barrier for hole injection from Gr to DP is estimated to be ≈ 1.0 eV (see discussion in the Supporting Information). This indicates that no hot-hole injection is expected for pump photon energies below 2.8 eV, which contradicts our observation. As such, in-gap defect states with much lower injection barriers are expected to play a critical role as the hole acceptors for below-E_g excitation. To confirm the hole transfer from Gr to the defect states in the DP, we conducted TA spectroscopy on the heterostructure upon 1.55 eV photoexcitation. As shown in Figure S10, we observe no photo-induced change across the whole spectrum, so that charge carrier population in the electronic bands can be ruled out. Together with our THz study, these results provide direct evidence of the key role of defects in hosting the injected holes. Such a defect-assisted mechanism is in line with a previous report revealing the intrinsic p-type conductivity likely arising from the Ag vacancy-induced shallow defect states; other types of in-gap empty states can populate as well, including Bi vacancy and Ag_{Bi} antisites.[32] Following

static interfacial CT, the filled defects and other initial shallow defects (filled defect states close to the valence band, if any) can serve as hole acceptors for the CT.

We further note that the switched hole injection direction by exciting the heterostructure across the E_g also leads to different charge recombination pathways and thus lifetimes. A clear recombination time increase from ≈ 100 ps for below-E_g excitation to over 1 ns for above-E_g excitation is observed. In both excitation and hole-transfer regimes, the recombination time is found to be pump energy and fluence independent. This observation is in clear contrast to the CT dynamics at Gr/TMDs interfaces. There, although the CT efficiency and pathways are modulated by the excitation energy, the final charge separation state, and thus the recombination lifetime, is observed to be identical throughout the whole excitation range.[8]

2.3. The Energetics of Hot Holes Impact on the Hole-Transfer Efficiency

After establishing the optical switching of the hole-transfer processes at DP/Gr interfaces, we investigate the effect of pump photon energy (i.e. the energetics of the hot carriers) by tuning the excitation wavelength in dictating the hole-transfer efficiency. Based on Figure 4b,c, it is clear that the hole-transfer efficiency is much enhanced as the photon energy increases for both below- and above-E_g photoexcitation. These results provide strong evidence of a hot-carrier-involved CT process. For below-E_g excitation, by increasing the pump photon energy from 1.20 to 2.07 eV, the hole- transfer efficiency is boosted by almost an order of magnitude. The enhanced hot-hole-transfer efficiency with increasing hot-hole energetics can be qualitatively understood as a combined consequence of the enhanced hot-hole-transfer rate (due to the enhanced driving force and the coupling strength for CT),[33] and the reduced hot-carrier relaxation rate from the initial energetics to below the CT energy barrier.[30,34] For above-E_g excitation, that is, when the holes are mainly generated in the DP, besides the favorable rate competition for ho-hole injection (e.g., enhanced driving force and the coupling strength for CT[33]), the

**ADVANCED
SCIENCE NEWS**

www.advancedsciencenews.com

**ADVANCED
MATERIALS**

www.advmat.de

recently reported much enhanced hot-hole-transport properties (e.g., enhanced mobility[25]) could favor the hot-carrier diffusion toward the interface for charge separation at DP/Gr interfaces.

Finally, to quantitatively assess the CT efficiencies for both below- and above-bandgap photoexcitation, we conduct time-domain THz spectroscopy at the time scales where the charge separation reaches a quasi-equilibrium state following CT (see details in the Supporting Information). Based on this measurement, we extract the frequency-resolved photoconductivity, which is dominated by the Gr's free carrier response. Using the Drude model to describe the data, we extract the carrier density change ΔN in Gr with and without photoexcitation (or CT). The absolute CT efficiency, defined as the ratio of the transferred carrier density ($\Delta N = N_{pump} - N_0$) to the absorbed photon density N_{abs}: $\eta = \Delta N / N_{abs}$, is therefore obtained. For 3.10 eV excitation, we estimate an $\approx 1.4\%$ hole-transfer efficiency from DP to Gr. Note that the estimated CT efficiency here represents the lower boundary as we assumed 100% photon-to-charge carrier generation quantum yield. This leads to an underestimation of CT efficiency. We further provided an estimation of the upper-limit CT efficiency to be 50% by assuming the transfer of free carriers dominates the interfacial CT (see more discussion in the Supporting Information). Based on the first-order approximation, that is, the CT quantum efficiency is proportional to the relative CT efficiency shown in Figure 4c, we estimate the highest CT efficiency for below-bandgap excitation at ≈ 2 eV to be around 8.4%.

3. Conclusion

Full optical control of the hole-transfer direction and recombination processes has been achieved in strongly coupled DP/Gr heterostructures by simply tuning the excitation photon energy. We unveiled the vital role of in-gap unfilled defect states and pump photon energy in tuning the interfacial hole-transfer processes. We find that the photoinjected "nascent" hot holes in Gr can be injected into in-gap defects of DP for below-E_g excitation while hole transfer from the valence band of the DP to the valence band of Gr occurs for above-E_g excitation. We provide experimental evidence that increasing the excitation photon energy leads to enhancement in interfacial hole-transfer efficiency for both below- and above-bandgap excitation regimes, demonstrating the critical role of excess hot-hole energy in enhancing interfacial CT. Our results not only unveil fundamental photophysics governing interfacial CT, but also provide a new method for controlling CT across DP/Gr heterostructures in optoelectronic applications (e.g., broadband photodetectors covering the THz up to the X-ray spectral range). In addition, the intriguing optical switching of hole transfer endows DP/Gr heterostructures with a new degree of freedom for, for example, manipulating the local gating field for new functionalities such as an optically induced memory effect in Gr.

4. Experimental Section

Sample Preparation: The DP/Gr heterostructure was prepared by first wet-transferring a CVD monolayer Gr onto FS, and then the Gr surface was treated by UV–ozone for 30 min. Finally, the DP solution was spin-coated on Gr to construct the DP/Gr heterostructures. A 0.5 solution of millimeter-sized $Cs_2AgBiBr_6$ single crystals[20,25] in dimethyl sulfoxide was spin-coated on top of the Gr layer on the FS substrate resulting in a uniform coverage with a thickness of ≈ 200 nm.

Optical Pump–THz Probe Spectroscopy: The OPTP setup was driven by a commercial, regenerative amplified, mode-locked Ti:sapphire femtosecond laser with a central wavelength of 800 nm, a pulse duration of 50 fs, and a repetition rate of 1 kHz. In the OPTP measurement, the sample was first pumped with different photon wavelengths generated via either a BBO crystal or a commercial optical parametric amplifier (OPA) from Light Conversion. After a pump–probe delay time t_P, the THz pulse propagated collinearly with the pump pulse and transmitted through the sample. The single-cycle THz pulse was generated from an 800 nm pulse by optical rectification in a 1 mm-thick ZnTe crystal. The transmitted THz electric field waveform $E(t)$ was detected coherently in a second ZnTe crystal by another 800 nm sampling pulse via the electro–optic effect. The photoconductivity dynamics $\Delta\sigma(t_P)$ of the sample was thus obtained by reading out the pump-induced relative change of THz peak electric field $-\Delta E/E_0$ as a function of t_P: $\Delta\sigma \approx -\Delta E/E_0$. $-\Delta E/E_0$ is proportional to $\Delta\sigma$ ($= \sigma_{pump} - \sigma_0$).

THz Time-Domain Spectroscopy: THz time-domain spectroscopy was conducted to obtain the frequency-resolved photoconductivity spectra. Instead of only recording the change of THz peak electric field after the photoexcitation, one can map the entire THz waveform with ($E_{pump}(t)$) and without ($E_0(t)$) optical excitation (and thus their difference $\Delta E(t) = E_{pump}(t) - E_0(t)$) at a fixed pump-sampling delay time by moving the optical delay lines for the pump beam and sampling beam simultaneously. By Fourier transformation of $E_0(t)$ and $\Delta E(t)$, the complex photoconductivity spectra $\sigma(\omega)$ were achieved following:

$$\sigma(\omega) = \frac{n_1 + n_2}{Z_0 \cdot l} \cdot \left[-\frac{\Delta E(\omega)}{E_0(\omega)} \right] \quad (1)$$

where n_1 and n_2 are the refractive indices in front of and behind the sample. Z_0 is the free space impedance. l is the thin film thickness (≈ 200 nm for all films in this study).

Transient Absorption Spectroscopy: A Yb-KGW oscillator (Light Conversion, Pharos SP) was used to produce 180 fs photon pulses with a wavelength of 1028 nm and at a repetition rate of 5 kHz. The pump beam was obtained by sending the fundamental beam through an OPA equipped with a second harmonic 12 module (Light Conversion, Orpheus), performing non-linear frequency mixing and producing an output beam whose wavelength could be tuned in the 310–1330 nm window. A small fraction of the fundamental beam power was used to produce a broadband probe spectrum (480–1600 nm), by supercontinuum generation in a sapphire crystal. The pump beam was transmitted through a mechanical chopper operating at 2.5 kHz. Pump and probe beam overlapped at the sample position with a small angle ($\approx 8°$), and with a relative time delay controlled by an automated delay stage. After transmission through the sample, the pump beam was dumped while the probe was collected on a detector (Ultrafast Systems, Helios). The differential absorbance was obtained via $\Delta A = \log(I_{on}/I_{off})$, I was the probe light incident on the detector with either pump on or pump off. TA data were corrected for probe-chirp via a polynomial correction to the coherent artifact.

Supporting Information

Supporting Information is available from the Wiley Online Library or from the author.

Acknowledgements

**ADVANCED
SCIENCE NEWS**

www.advancedsciencenews.com

**ADVANCED
MATERIALS**

www.advmat.de

Conflict of Interest

The authors declare no conflict of interest.

Author Contributions

H.I.W. and E.D. designed and supervised the project. H.Z. conducted Raman and THz measurements. E.D. synthesized the $Cs_2AgBiBr_6$ perovskites and prepared the heterostructures. S.F. prepared the graphene monolayers on the substrates. M.C.R.G. conducted KPFM measurements under the supervision of S.D.F. I.d.F. and J.J.G. conducted TA measurements under the supervision of A.J.H. L.G. conducted photoconductivity measurements and X.Y. measured the Raman studies on the D-band evolution on UV–ozone-treated graphene samples. All authors discussed and analyzed the results. H.Z. and H.I.W. drafted the paper with the input from all authors. All authors have given approval to the final version of the manuscript.

Data Availability Statement

The data that support the findings of this study are available from the corresponding author upon reasonable request.

[1] X. Du, I. Skachko, A. Barker, E. Y. Andrei, *Nat. Nanotechnol.* **2008**, *3*, 491.

[2] L. Banszerus, M. Schmitz, S. Engels, M. Goldsche, K. Watanabe, T. Taniguchi, B. Beschoten, C. Stampfer, *Nano Lett.* **2016**, *16*, 1387.

[3] F. H. Koppens, T. Mueller, P. Avouris, A. C. Ferrari, M. S. Vitiello, M. Polini, *Nat. Nanotechnol.* **2014**, *9*, 780.

[4] G. Konstantatos, M. Badioli, L. Gaudreau, J. Osmond, M. Bernechea, F. P García de Arquer, F. Gatti, F. H. Koppens, *Nat. Nanotechnol.* **2012**, *7*, 363.

[5] Z. Liu, H. Qiu, S. Fu, C. Wang, X. Yao, A. G. Dixon, S. Campidelli, E. Pavlica, G. Bratina, S. Zhao, L. Rondin, J. S. Lauret, A. Narita, M. Bonn, K. Mullen, A. Ciesielski, H. I. Wang, P. Samori, *J. Am. Chem. Soc.* **2021**, *143*, 17109.

[6] W. Zhang, C. P. Chuu, J. K. Huang, C. H. Chen, M. L. Tsai, Y. H. Chang, C. T. Liang, Y. Z. Chen, Y. L. Chueh, J. H. He, M. Y. Chou, L. J. Li, *Sci. Rep.* **2014**, *4*, 3826.

[7] X. Wang, Z. Cheng, K. Xu, H. K. Tsang, J.-B. Xu, *Nat. Photonics* **2013**, *7*, 888.

[8] S. Fu, I. du Fossé, X. Jia, J. Xu, X. Yu, H. Zhang, W. Zheng, S. Krasel, Z. Chen, Z. M. Wang, *Sci. Adv.* **2021**, *7*, eabd9061.

[9] M. Massicotte, P. Schmidt, F. Vialla, K. Watanabe, T. Taniguchi, K. J. Tielrooij, F. H. Koppens, *Nat. Commun.* **2016**, *7*, 12174.

[10] C. Trovatello, G. Piccinini, S. Forti, F. Fabbri, A. Rossi, S. De Silvestri, C. Coletti, G. Cerullo, S. D. Conte, *npj 2D Mater. Appl.* **2022**, *6*, 8.

[11] J. Jeong, M. Kim, J. Seo, H. Lu, P. Ahlawat, A. Mishra, Y. Yang, M. A. Hope, F. T. Eickemeyer, M. Kim, Y. J. Yoon, I. W. Choi, B. P. Darwich, S. J. Choi, Y. Jo, J. H. Lee, B. Walker, S. M. Zakeeruddin, L. Emsley, U. Rothlisberger, A. Hagfeldt, D. S. Kim, M. Gratzel, J. Y. Kim, *Nature* **2021**, *592*, 381.

[12] H. Min, D. Y. Lee, J. Kim, G. Kim, K. S. Lee, J. Kim, M. J. Paik, Y. K. Kim, K. S. Kim, M. G. Kim, T. J. Shin, S. Il Seok, *Nature* **2021**, *598*, 444.

[13] Y. Lee, J. Kwon, E. Hwang, C. H. Ra, W. J. Yoo, J. H. Ahn, J. H. Park, J. H. Cho, *Adv. Mater.* **2015**, *27*, 41.

[14] P. H. Chang, S. Y. Liu, Y. B. Lan, Y. C. Tsai, X. Q. You, C. S. Li, K. Y. Huang, A. S. Chou, T. C. Cheng, J. K. Wang, C. I. Wu, *Sci. Rep.* **2017**, *7*, 46281.

[15] E. T. McClure, M. R. Ball, W. Windl, P. M. Woodward, *Chem. Mater.* **2016**, *28*, 1348.

[16] W. Pan, H. Wu, J. Luo, Z. Deng, C. Ge, C. Chen, X. Jiang, W.-J. Yin, G. Niu, L. Zhu, L. Yin, Y. Zhou, Q. Xie, X. Ke, M. Sui, J. Tang, *Nat. Photonics* **2017**, *11*, 726.

[17] J. A. Steele, W. Pan, C. Martin, M. Keshavarz, E. Debroye, H. Yuan, S. Banerjee, E. Fron, D. Jonckheere, C. W. Kim, W. Baekelant, G. Niu, J. Tang, J. Vanacken, M. Van der Auweraer, J. Hofkens, M. B. J. Roeffaers, *Adv. Mater.* **2018**, *30*, 1804450.

[18] A. H. Slavney, T. Hu, A. M. Lindenberg, H. I. Karunadasa, *J. Am. Chem. Soc.* **2016**, *138*, 2138.

[19] R. L. Z. Hoye, L. Eyre, F. Wei, F. Brivio, A. Sadhanala, S. Sun, W. Li, K. H. L. Zhang, J. L. MacManus-Driscoll, P. D. Bristowe, R. H. Friend, A. K. Cheetham, F. Deschler, *Adv. Mater. Interfaces* **2018**, *5*, 1800464.

[20] M. Keshavarz, E. Debroye, M. Ottesen, C. Martin, H. Zhang, E. Fron, R. Küchler, J. A. Steele, M. Bremholm, J. Van de Vondel, H. I. Wang, M. Bonn, M. B. J. Roeffaers, S. Wiedmann, J. Hofkens, *Adv. Mater.* **2020**, *32*, 2001878.

[21] M. Delor, A. H. Slavney, N. R. Wolf, M. R. Filip, J. B. Neaton, H. I. Karunadasa, N. S. Ginsberg, *ACS Energy Lett.* **2020**, *5*, 1337.

[22] A. C. Ferrari, D. M. Basko, *Nat. Nanotechnol.* **2013**, *8*, 235.

[23] A. Das, S. Pisana, B. Chakraborty, S. Piscanec, S. K. Saha, U. V. Waghmare, K. S. Novoselov, H. R. Krishnamurthy, A. K. Geim, A. C. Ferrari, A. K. Sood, *Nat. Nanotechnol.* **2008**, *3*, 210.

[24] X. Jia, M. Hu, K. Soundarapandian, X. Yu, Z. Liu, Z. Chen, A. Narita, K. Mullen, F. H. L. Koppens, J. Jiang, K. J. Tielrooij, M. Bonn, H. I. Wang, *Nano Lett.* **2019**, *19*, 9029.

[25] H. Zhang, E. Debroye, W. Zheng, S. Fu, L. D. Virgilio, P. Kumar, M. Bonn, H. I. Wang, *Sci. Adv.* **2021**, *7*, eabj9066.

[26] X. Yu, S. Fu, M. Mandal, X. Yao, Z. Liu, W. Zheng, P. Samori, A. Narita, K. Mullen, D. Andrienko, M. Bonn, H. I. Wang, *J. Chem. Phys.* **2022**, *156*, 074702.

[27] G. Jnawali, Y. Rao, H. Yan, T. F. Heinz, *Nano Lett.* **2013**, *13*, 524.

[28] S. F. Shi, T. T. Tang, B. Zeng, L. Ju, Q. Zhou, A. Zettl, F. Wang, *Nano Lett.* **2014**, *14*, 1578.

[29] A. Tomadin, S. M. Hornett, H. I. Wang, E. M. Alexeev, A. Candini, C. Coletti, D. Turchinovich, M. Kläui, M. Bonn, F. H. Koppens, *Sci. Adv.* **2018**, *4*, eaar5313.

[30] E. A. A. Pogna, X. Jia, A. Principi, A. Block, L. Banszerus, J. Zhang, X. Liu, T. Sohier, S. Forti, K. Soundarapandian, B. Terrés, J. D. Mehew, C. Trovatello, C. Coletti, F. H. L. Koppens, M. Bonn, H. I. Wang, N. van Hulst, M. J. Verstraete, H. Peng, Z. Liu, C. Stampfer, G. Cerullo, K.-J. Tielrooij, *ACS Nano* **2021**, *15*, 11285.

[31] G. Jnawali, Y. Rao, J. H. Beck, N. Petrone, I. Kymissis, J. Hone, T. F. Heinz, *ACS Nano* **2015**, *9*, 7175.

[32] Z. Xiao, W. Meng, J. Wang, Y. Yan, *ChemSusChem* **2016**, *9*, 2628.

[33] H. I. Wang, I. Infante, S. T. Brinck, E. Canovas, M. Bonn, *Nano Lett.* **2018**, *18*, 5111.

[34] B. Gao, G. Hartland, T. Fang, M. Kelly, D. Jena, H. G. Xing, L. Huang, *Nano Lett.* **2011**, *11*, 3184.